35th Annual International Conference of the IEEE EMBS
Osaka, Japan, 3 - 7 July, 2013

A Bilayer Representation of the Human Atria

Edward Vigmond[1,2], Simon Labarthe[1,2,3], Hubert Cochet[1,4], Yves Coudiere[1,2,3], Jacques Henry[1,2,3], Pierre Jaïs[1,4]

Abstract— **Atrial fibrillation is the most commonly encountered clinical arrhythmia. Despite recent advances in treatment by catheter ablation, its origin is still incompletely understood and it may be difficult to treat. Computer modelling offers an attractive complement to experiment. Simulations of fibrillation, however, are computationally demanding since the phenomenon requires long periods of observation. Because the atria are thin walled structures, they are often modelled as surfaces. However, this may not always be appropriate as the crista terminalis and pectinate muscles are discrete fibrous structures lying on the endocardium and cannot be incorporated into the surface. In the left atrium, there are essentially two layers with an abrupt change in fibre orientation between them. We propose a double layer method, using shell elements to incorporate wall thickness, where fibre direction is independent in each layer and layers are electrically linked. Starting from human multi-detector CT (MDCT) images, we extracted surfaces for the atria and manually added a coronary sinus. Propagation of electrical activity was modelled with the monodomain equation. Results indicate that major features are retained while reducing computation cost considerably. Meshes based on the two layer approach will facilitate studies of AF.**

I. INTRODUCTION

Atrial fibrillation is the most commonly encountered clinical arrhythmia. Despite recent advances in treatment by catheter ablation, its origin is still incompletely understood and it often proves difficult to treat. Computer modelling offers an attractive complement to experiment.

Since the atria are thin walled structures, they are often considered as surfaces. However, this may not always be appropriate as the endocardium is better described as a fibrous network which lines a smoother epicardium. In the right atrium (RA), the crista terminalus (CT) and pectinate muscles (PM) are large distinct endocardial fibres. In the left atrium (LA), there is an abrupt change in fibre orientation between the epicardial and endocardial layers. The layers may be weakly coupled electrically since several studies have measured dissociation of activity between them [1], [2].

Many different geometrical atrial models have been built, indicating the importance of atrial geometry on atrial propagation. Surface models [3] have the advantage of fast computation but may not capture the dissociated activity. Models with wall thickness have been constructed using finite elements [4], finite volumes [5], finite differences [6] and cables [7]. While these models offer a more complete description, they can quickly increase the computational load especially for larger human hearts.

Simulations of fibrillation are computationally demanding since the phenomenon requires long periods of observation. As a compromise between the surface and three dimensional approach, we propose a two layer approach with discrete connections between the layers. To further mitigate differences with full 3D models, we also propose using shell elements which allow associating a different thickness with each element. In this paper, we describe the model and demonstrate propagation.

II. METHODS

A. Geometrical mesh

1) Imaging the atria: Biatrial geometry was acquired in vivo using ECG-gated contrast-enhanced multi-detector computed tomography in a patient with no history of atrial disorder. Imaging was performed using a 64-slice scanner (SOMATOM Definition, Siemens Medical Solutions, Forchheim, Germany) during the intravenous injection of a 120 mL bolus of iodinated contrast agent at the rate of 4 mL s^{-1}. ECG-gating was set with the acquisition window occurring at end-systole, when atrial motion is minimal. Acquisition parameters were a slice thickness of 0.5 mm, a tube voltage of 120 kV, a maximum tube current of 850 mAs, and a gantry rotation time of 330 ms. An imaging volume comprising the whole atria was reconstructed with a voxel size of 0.5 mm x0.4 mmx0.4 mm. Trans-axial images were imported in DICOM format into a local database of the software OsiriX 3.6.1 (OsiriX foundation, Geneva, Switzerland). The endocardial surface was segmented automatically using region growth segmentation. Volume rendering reconstructions were used to remove non atrial structures from the segmentation. Pulmonary veins were cut several centimetres from their ostia since myocardium is known to extend up to 2 centimeters beyond the pulmonary vein ostia [8]. The resulting segmentation was used to compute a 3D mesh in vtk format using the software CardioviZ3D (INRIA Asclepios, Sophia Antipolis, France). The mesh was smoothed with weighted Laplacian smoothing and optimized with the software freeYams to get a mesh suitable for calculation that contained 361483 nodes and 715034 elements with a mean diameter of 0.492 mm.

2) Fibre definition: The fibre structure was defined with a rule-based semi-automatic method [9] based on two atrial characteristics : (1) atrial geometry can be divided into basic

The corresponding author is E. Vigmond edward.vigmond@u-bordeaux1.fr

The research leading to these results has received funding from the European Union Seventh Framework Programme (FP7/2007-2013) under Grant Agreement HEALTH-F2-2010-261057

[1] Institut LIRYC, Pessac, France
[2] Lab IMB, University of Bordeaux 1, Talence, France
[3] INRIA Bordeaux Sud Ouest, Talence, France
[4] Equipex MUSIC, CHU / Universit de Bordeaux / INSERM U1045, Pessac, France

978-1-4577-0216-7/13/$26.00 ©2013 IEEE

cylindrical structures with circumferential fibre orientation, and (2) the fibre arrangement is continuous. The atrial mesh was first manually decomposed into cylinder-like elements. Local circumferential structure was semi-automatically obtained by determining the axis as an eigenvector of the inertia tensor. Finally, an in-painting algorithm extended the fibre direction continuously on to the whole geometry.

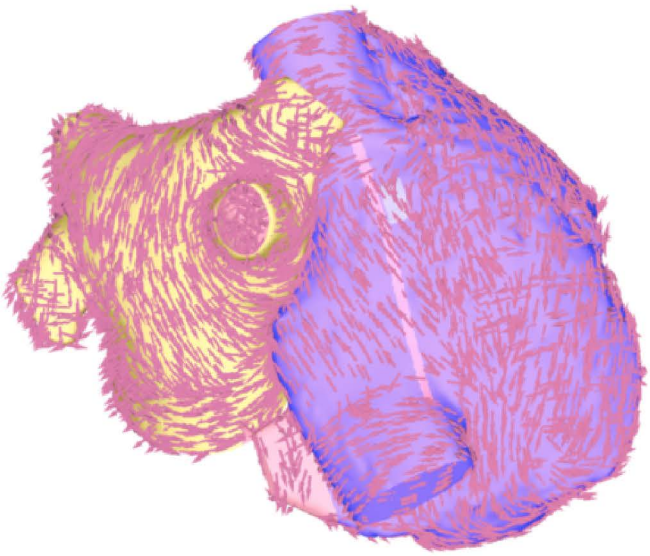

Fig. 1. Superio-posterior view of left free wall of atria showing fibre orientation.

3) Manual mesh completion: Small structures that were partially acquired were manually constructed with the following workflow : the points of insertion of the new structure in the mesh were identified. Plane surfaces connecting those points were defined and meshed with the software Gmsh. The structure was then smoothed by a Laplacian method with the software MeshLab (3D-CoForm Project, Italy).

4) Main modelling options: In order to describe the atria as a bilayer structure, we needed to assume some physiological modelling options a priori, especially focusing on transmural heterogeneities.

a) Right Atria: According to histological descriptions of the atria [10], the RA can be seen as a monolayer structure, except in the appendage (RAA) and in the roof where the CT and the PM bring thickness and fibrous inhomogeneities. A first layer modeled the epicardium of the RA including its main fibre structures : the circular fibres that surround the superior vena cava crossed the CT and covered the RAA to blend with the circular bundle of the vestibule. A second layer was applied at the location of PM and the CT in order to include the longitudinal fibre direction along those structures in the endocardial part of the RA. A poor conduction zone was introduced along the left side of the sinoatrial node (SAN) [11]

b) Left Atria (LA): The left atrium (LA) fibre structure can be described as a two layer geometry. The main transmural heterogeneities are concentrated in the anterior wall and on the pulmonary veins (PV). The circumferential and oblique fibres of the anterior epicardium blend with Bachmann's bundle (BB) whereas the endocardial fibres of the septoatrial bundle run from the vestibule to the dome of the LA. The fibre structure of the LA can show strong discontinuities with a nonuniform arrangement and orthogonal transmural variations of fibres directions. Those characteristics were attentively reproduced in the two layers of the LA.

c) Transseptal connexions: The LA and RA were electrically insulated and interconnected by the three main interatrial connexions: the BB, the fossa ovalis (FO) and the coronary sinus (CS). The BB was segmented manually as a 3D structure and reduced to two surfaces : the first one laid on the posterior face of the BB and inserted into the septal wall of LA while the second one was constructed as a mean surface of the volumetric structure and blended into the septopulmonary bundle of the LA. The FO and the CS were identifiable after the segmentation step and connected manually from RA to LA.

B. Electrophysiological model

The monodomain equation was used to describe the propagation of electrical conductivity

$$\nabla \cdot \overline{\sigma}_i \nabla V_m = \beta \left(C_m \frac{\partial V_m}{\partial t} + I_{\text{ion}}(V_m, t, \bar{\zeta}) \right) \qquad (1)$$

where V_m is the transmembrane voltage (mV), $\overline{\sigma}_i$ is the conducitivity tensor ($\mathrm{S\,m^{-1}}$), β is the ratio of membrane surface to volume in which it is contained ($0.14\ \mu\mathrm{m^{-1}}$), C_m is the membrane capacitance ($1.0\ \mu\mathrm{F\,cm^{-2}}$), and I_{ion} is the transmembrane current which is a function of voltage, time, and $\bar{\zeta}$, a set of state variables. The ionic model used was the Courtemanche human atrial action potential model [12]. Sodium conductance was increased by a factor of four from the published value to achieve realistic propagation speeds. Conductivity values were further adjusted to give realistic activation times: $(0.3, 0.04)\mathrm{S\,m^{-1}}$ for longitudinal and transverse conduction, except in the PM and CT where longitudinal conduction was set to $1.0\mathrm{S\,m^{-1}}$.

A structural block zone was implemented close to the SAN as found experimentally [11]. In this region a passive ionic model was used with a resting level -80 mV and intracellular conductivity was reduced by a factor of 100. The SAN is located between the block zone and the CT. Accordingly, a small region here was stimulated with a transmembrane current to simulate the site of first SAN excitation.

The equations were solved using the finite element method. To account for changes in thickness over a surface, linear triangular shell elements were chosen. These elements assume a thickness across which activity is uniform. Connections between surfaces were implemented as one dimensional linear finite elements. 134510 line elements were required to couple the surfaces together. The system was solved by the CARP cardiac simulator [13] with a fixed time step of 25 μs using a Crank-Nicolson approach to solve Eq. 1. On a desktop workstation with Intel(R) Xeon X5650 CPUs running at 2.67GHz, it took seven seconds to simulate one

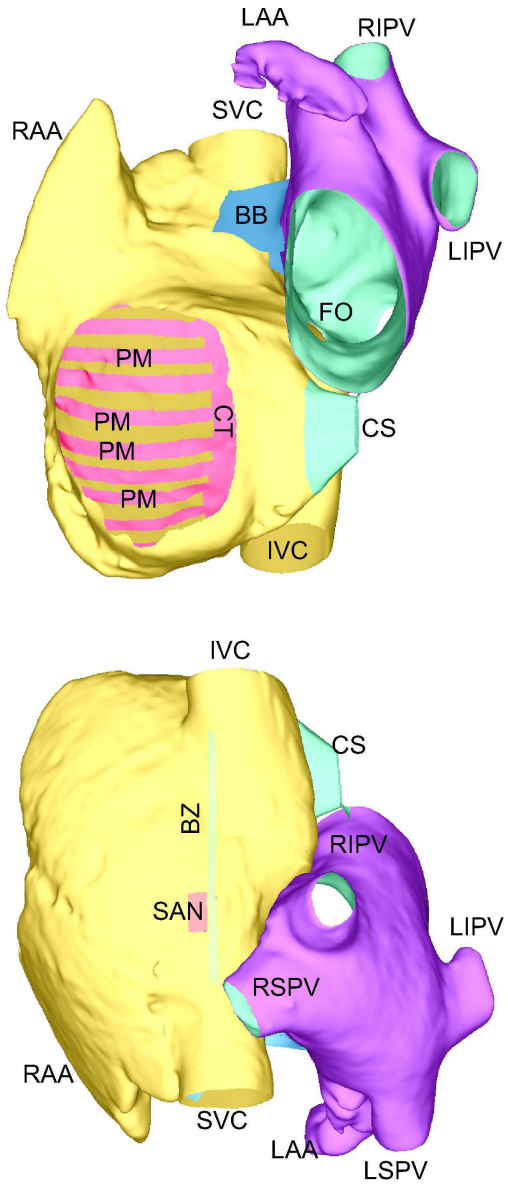

Fig. 2. Top: Inferior view of the atria. Bottom: Superior view. All distinct surfaces are colored uniquely. SVC-superior vena cava. IVC-inferior vena cava. BB-Bachmann's bundle. CS- coronary sinus. BZ-block zone. SAN-sinoatrial node. RSPV-right superior pulmonary vein. RIPV-right inferior pulmonary vein.LSPV-left superior pulmonary vein. LIPV-left inferior pulmonary vein. RAA-right atrial appendage. LAA-left atrial appendage. CT-crista terminalis. PM- pectinate muscles.

ms on ten cores, while on a desktop computer with an NVidia Quadro 4000 (256 cores) it took 18 seconds per millisecond running on the GPU.

III. RESULTS

A. FEM Validation

Two simple examples were run to confirm the correctness of the shell elements. In the first test, a 2 cm long $\times$ 100 μm wide strand was divided into two sections, one with a depth of 100 μm, and the other with a depth of 1000 μm. Results are shown in Fig. 3. Propagation across the interface was successful if the thick portion of the strand was stimulated but not if the thin portion was stimulated. For the second test, the depth of a 2 cm long$\times$ 100 μm wide strand was linearly tapered from 100 to 1000 μm. See Fig 4. Stimulating at the thin end resulted in a propagation velocity of 708 mm/s with a delayed activation compared to stimulating the thick end which resulted in a propagation velocity of 726 mm/s.

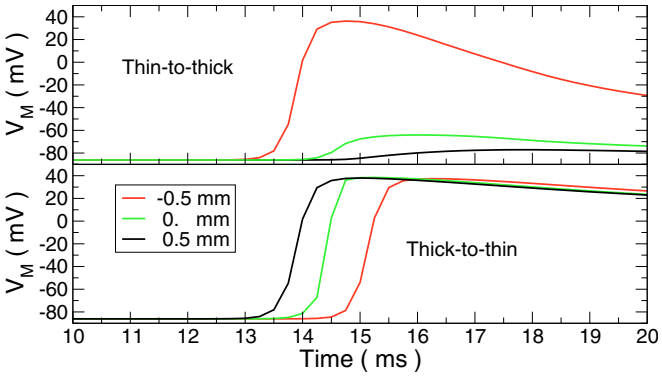

Fig. 3. Transmembrane voltage measured near the junction of thick and thin segments. Propagation was initiated at the thin end (top) or the thick end (bottom). Curves obtained at different distances from the junction are indicated.

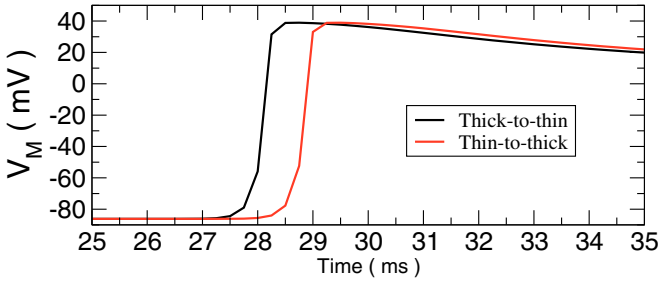

Fig. 4. Transmembrane voltage measured at terminal end of a tapering cable. Propagation was initiated at the thin end or the thick end.

B. Activation times

A normal sinus activation pattern was produced with a total activation time on the order of 190 ms. Sinus activation was simulated by stimulating a region corresponding to the physical location of the SAN. The block zone delayed propagation towards the septum as activity had to go around it. Activity was faster along the CT and PM than in the overlying muscle. Activity entered the large muscle bundles and then raced ahead of the epicardial activity, pulling it along. Propagation across BB provided the first transseptal activation. Activity crossed the FO a short time later and merged in the LA with the wavefront from originating from BB. Activity along the CS was the last to cross from right to left. The LAA was the last portion of the model excited.

A comparison was made between the bilayer and monolayer models. For the monolayer model, the CT, PM, and endocardial LA were removed. The activation map was computed and differenced with bilayer model in Fig. 5. The effect of the RA endocardial muscle bundles are clearly seen, with the dark blue indicating slower conduction without

the second layer. In the LA, the additional muscle layer complicated propagation, causing some parts to be delayed (in red) and other parts to be activated sooner (in blue).

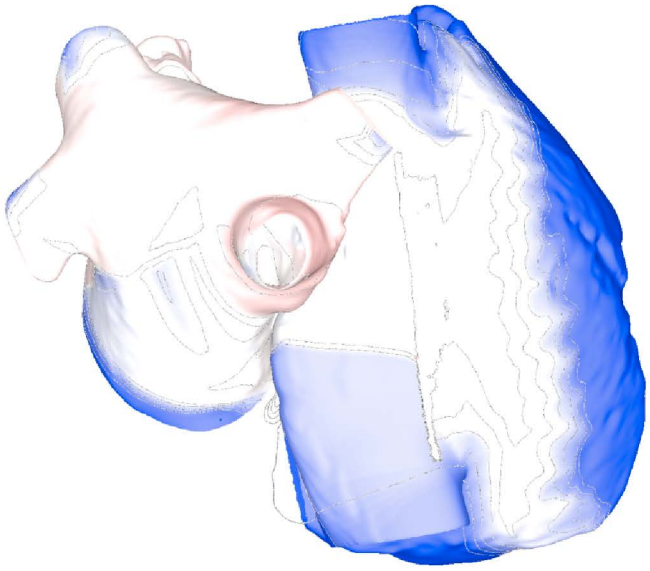

Fig. 5. Difference in activation times for monoloayer and bilayer atrial models. Colors indicate the activation time differences of the monoloayer compared to the bilayer with colors ranging from -10 ms (dark blue) to red (+10 ms). 2 ms isodifference lines are shown.

IV. DISCUSSION

We presented a method for reducing the computation required for atrial electrophysiological modelling while still retaining the ability to implement fine changes. A two sheet approach has been used previously, but not with a realistic geometry [14]. The study did reinforce the notion that dissociation between layers is important for describing atrial activity during fibrillation. With realistic, image derived, geometrical information, our model will be able to better identify regions that are targets for preventing fibrillation.

This model is unique in that it used shell elements to be able to assign different thicknesses to different parts of each layer. When the thickness was changed in the test strand, the behavior was as expected. When a wave propagates from a thinner strand to a thicker one, a larger load is imposed and it is harder to excite the thicker tissue. If the change in thickness is great enough, propagation may fail. The same effect could be seen from a full 3D model, but given element spacing on the order of 300 micrometers and a wall thickness of at least 3 mm, modelling the thickness would require at least an order of magnitude increase in the number of nodes.

Future work will involve setting appropriate thicknesses for all elements, adjusting action potential durations over the entire model, and further refining the SAN in light of the recent work of Fedorov [11]. In particular, the CT needs to form another block zone and exit points need to be defined.

This model can be a valuable tool for studying atrial arrhythmias as well as for looking at ablation strategies in patient specific meshes. It significantly reduces computation time while retaining detailed features affecting propagation.

Acknowledgements: The research leading to these results has received funding from the European Union Seventh Framework Programme (FP7/2007-2013) under Grant Agreement HEALTH-F2-2010-261057

REFERENCES

[1] K. Derakhchan, D. Li, M. Courtemanche, B. Smith, J. Brouillette, P. L. Pag, and S. Nattel, "Method for simultaneous epicardial and endocardial mapping of in vivo canine heart: application to atrial conduction properties and arrhythmia mechanisms." *J Cardiovasc Electrophysiol*, vol. 12, no. 5, pp. 548–555, May 2001.

[2] J. Eckstein, B. Maesen, D. Linz, S. Zeemering, A. van Hunnik, S. Verheule, M. Allessie, and U. Schotten, "Time course and mechanisms of endo-epicardial electrical dissociation during atrial fibrillation in the goat." *Cardiovasc Res*, vol. 89, no. 4, pp. 816–824, Mar 2011. [Online]. Available: http://dx.doi.org/10.1093/cvr/cvq336

[3] P. Ruchat, L. Dang, N. Virag, J. Schlaepfer, L. K. von Segesser, and L. Kappenberger, "A biophysical model of atrial fibrillation to define the appropriate ablation pattern in modified maze." *Eur J Cardiothorac Surg*, vol. 31, no. 1, pp. 65–69, Jan 2007. [Online]. Available: http://dx.doi.org/10.1016/j.ejcts.2006.10.015

[4] G. Seemann, C. Hper, F. B. Sachse, O. Dssel, A. V. Holden, and H. Zhang, "Heterogeneous three-dimensional anatomical and electrophysiological model of human atria." *Philos Transact A Math Phys Eng Sci*, vol. 364, no. 1843, pp. 1465–1481, Jun 2006. [Online]. Available: http://dx.doi.org/10.1098/rsta.2006.1781

[5] D. Harrild and C. Henriquez, "A computer model of normal conduction in the human atria." *Circ Res*, vol. 87, no. 7, pp. E25–E36, Sep 2000.

[6] O. V. Aslanidi, M. A. Colman, J. Stott, H. Dobrzynski, M. R. Boyett, A. V. Holden, and H. Zhang, "3d virtual human atria: A computational platform for studying clinical atrial fibrillation." *Prog Biophys Mol Biol*, vol. 107, no. 1, pp. 156–168, Oct 2011. [Online]. Available: http://dx.doi.org/10.1016/j.pbiomolbio.2011.06.011

[7] M.-E. Ridler, M. Lee, D. McQueen, C. Peskin, and E. Vigmond, "Arrhythmogenic consequences of action potential duration gradients in the atria." *Can J Cardiol*, vol. 27, no. 1, pp. 112–119, 2011. [Online]. Available: http://dx.doi.org/10.1016/j.cjca.2010.12.002

[8] T. SAITO, K. WAKI, and A. E. BECKER, "Left atrial myocardial extension onto pulmonary veins in humans:," *Journal of Cardiovascular Electrophysiology*, vol. 11, no. 8, pp. 888–894, 2000. [Online]. Available: http://dx.doi.org/10.1111/j.1540-8167.2000.tb00068.x

[9] S. Labarthe, Y. Coudière, J. Henry, and H. Cochet, "A semi-automatic method to construct atrial fibre structures: a tool for atrial simulations," in *CinC 2012 - Computing in cardiology*, vol. 39, Krakow, Pologne, November 2012, pp. 881–4.

[10] S. Y. Ho, R. H. Anderson, and D. Sánchez-Quintana, "Atrial structure and fibres: morphologic bases of atrial conduction." *Cardiovasc Res*, vol. 54, no. 2, pp. 325–336, May 2002.

[11] V. V. Fedorov, R. B. Schuessler, M. Hemphill, C. M. Ambrosi, R. Chang, A. S. Voloshina, K. Brown, W. J. Hucker, and I. R. Efimov, "Structural and functional evidence for discrete exit pathways that connect the canine sinoatrial node and atria." *Circ Res*, vol. 104, no. 7, pp. 915–923, Apr 2009. [Online]. Available: http://dx.doi.org/10.1161/CIRCRESAHA.108.193193

[12] M. Courtemanche, R. J. Ramirez, and S. Nattel, "Ionic mechanisms underlying human atrial action potential properties: insights from a mathematical model." *Am J Physiol*, vol. 275, no. 1 Pt 2, pp. H301–H321, Jul 1998.

[13] E. J. Vigmond, M. Hughes, G. Plank, and L. J. Leon, "Computational tools for modeling electrical activity in cardiac tissue." *J Electrocardiol*, vol. 36 Suppl, pp. 69–74, 2003.

[14] A. Gharaviri, S. Verheule, J. Eckstein, M. Potse, N. H. L. Kuijpers, and U. Schotten, "A computer model of endo-epicardial electrical dissociation and transmural conduction during atrial fibrillation." *Europace*, vol. 14 Suppl 5, pp. v10–v16, Nov 2012. [Online]. Available: http://dx.doi.org/10.1093/europace/eus270